



# Efficient electrochemical detection of hazardous para-nitrophenol based on a carbon paste electrode modified with green synthesized gold/iron oxide nanocomposite

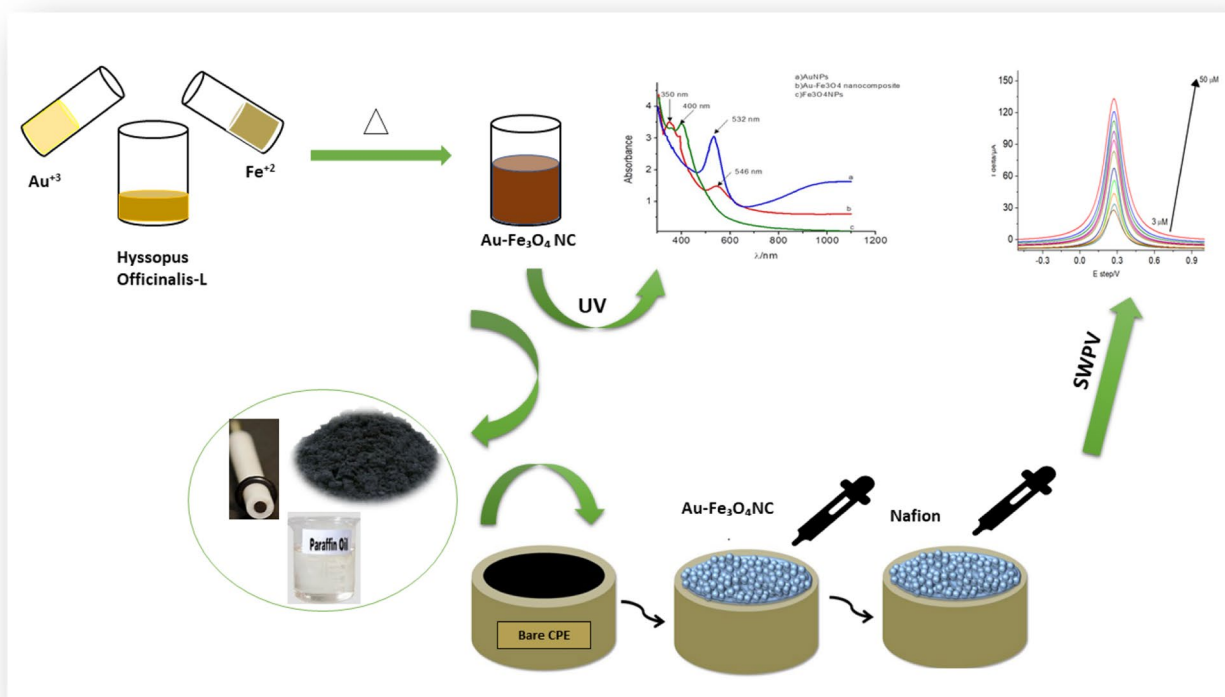
Aisha A. Ganash<sup>1</sup> · Rahmah A. Aljubairy<sup>1</sup>

Received: 24 November 2021 / Accepted: 16 January 2022 / Published online: 2 February 2022  
© Institute of Chemistry, Slovak Academy of Sciences 2022

## Abstract

In this study, a Au-Fe<sub>3</sub>O<sub>4</sub> nanocomposite-coated carbon paste electrode was developed as a simple, inexpensive, and efficient sensor for the removal and detection of para nitrophenol in acetate buffer solution (pH = 4.5). The Au-Fe<sub>3</sub>O<sub>4</sub> nanocomposite was green synthesized using Hyssopus Officinalis-L extract solution, and the fabricated nanocomposite was characterized by SEM, EDX, XRD, FTIR, UV–vis, and TEM analysis. The limit of detection (0.023 μM) in the concentration range (3–50 μM) was calculated at the optimum condition. The CPE/Au-Fe<sub>3</sub>O<sub>4</sub> nanocomposite electrode shows high selectivity, stability, and reproducibility with acceptable recovery (96–112%). Furthermore, the CPE/Au-Fe<sub>3</sub>O<sub>4</sub> nanocomposite electrode shows excellent catalytic activity for the reduction in para nitrophenol with a rate constant (*k*) of 0.01 min<sup>-1</sup> and correlation coefficient *R*<sup>2</sup> of 0.999.

## Graphical abstract



**Keywords** Au-Fe<sub>3</sub>O<sub>4</sub> nanocomposite · Green synthesis · Para nitrophenol · Catalytic activity

## Introduction

Phenol compounds and their derivatives are severe environmental pollutants, and most of them are used in drug, dyes, and pesticide formation (Tang et al. 2013). Nitrophenol toxic waste is adverse to the environment due to its stability for a long time (Busca et al. 2008). Para nitrophenol ( $\rho$ -NP) is an important compound that is used in the production of fungicides, plasticizers, dyes, pesticides, and explosives (Chen and Huang 2009). In recent years, the Environmental Protection Agency (EPA) has classified  $\rho$ -NP as one of the most polluting pollutants in the USA. A (Ebrahimzadeh et al. 2009; Li et al. 2013), the symptoms of  $\rho$ -NP poisoning are fever, death, headache, and breathing problems (Sittig 2021). Various committees limit the acceptable level of  $\rho$ -NP to 0.43  $\mu$ M (EPA) and 0.72 nM (European Commission) (Wei et al. 2011). Recently, different detection methods have been adopted to analyze  $\rho$ -NP, such as UV–vis spectroscopy (Lipczynska-Kochany 1991), liquid chromatography (Arbab Zavar et al. 2012), gas chromatography and optical spectroscopy (Niazi and Yazdanipour 2007; Guidotti et al. 1999; Wong et al. 1991; Mußmann et al. 1994; Thompson et al. 1996; Belloli et al. 1999), high-performance liquid chromatography (Hofmann et al. 2008) and high-performance capillary electrophoresis (Guo et al. 2004). Electrochemical techniques represent the most useful methods due to their rapid response, high sensitivity, high accuracy, low cost, and simple operation.

Metal nanoparticles have attracted great interest owing to their large surface area, excessive electrocatalytic activity, and good electrical conductivity (Jiao et al. 2013). Generally, nanocomposite materials, which involve different nanometals, have attracted increasing attention because of their mixed physical/chemical properties and their varied applications (Salgueiriño-Maceira et al. 2006; Feng et al. 2006; Yi et al. 2006; Roca and Haes 2008; Li et al. 2006; Caruso 2001). The application of nanocomposite metals is controlled by their structure, combination, distribution, and stability (Leung et al. 2012). Different methods of fabrication of the gold nanoparticles (AuNPs) and their application were reported (German et al. 2019, 2020, 2021; Ramaviciene et al. 2021, 2016; Khatoon et al. 2018). AuNPs have great applications in sensing methods in catalysis and biosensors (Jiao et al. 2013). Modified glassy carbon electrodes (GCEs) with AuNPs were adopted for electrochemical determination of dopamine and ascorbic acid at the same time (Hu et al. 2009). In 2011, Zhang et al. investigated the determination of nitrophenol using AuNPs/GCE (Chu et al. 2011). Jiao et al. reported a method for electrochemical reduction of  $\rho$ -NP using graphene/AuNPs/

GCE under optimum conditions, and a  $1 \times 10^{-8}$  M limit of detection was achieved (Jiao et al. 2013). As reported before, the nanostructure of the Au-Fe<sub>3</sub>O<sub>4</sub> nanocomposite can be classified into monodispersed and aggregate hybrid nanostructures (Leung et al. 2012). The synthesis of aggregate random polydispersed nanostructures is simple compared to monodispersed structures (Leung et al. 2012). Nakagawa et al. mixed presynthesized Fe<sub>3</sub>O<sub>4</sub> NPs and polyvinyl alcohol (PVA) with HAuCl<sub>4</sub>, followed by gamma radiation (Ca. 6 kGy) (Kojima et al. 2010; Kamei et al. 2009). In another study, Stayton et al. described the combination of Au and Fe<sub>3</sub>O<sub>4</sub> NPs using poly(N-isopropyl acrylamide) as a binding agent (Nash et al. 2010). Later, nanotechnology turned to use green biological methods for the fabrication of AuNPs and Fe<sub>3</sub>O<sub>4</sub> (Elemike et al. 2019). *Hyssopus officinalis*-L grows to two feet and is found in Europe and naturalized in England. The plant is used as a flavoring in salad and soups. It is used as an expectorant and tonic stomach, and it is used to remedy bronchitis and respiratory infection. The harvested plant was carried out when it had full flowers and could be dried for future use (Chevallier 1996; Grieve 1984).

Herein, AuNPs, Fe<sub>3</sub>O<sub>4</sub>NPs, and Au-Fe<sub>3</sub>O<sub>4</sub> nanocomposites were green synthesized using *Hyssopus Officinalis*-L, and the prepared nanocomposite was characterized using FTIR, UV–vis, SEM, EDX, XRD, and TEM analysis.

The nanocomposite was used to modify the carbon paste electrode (CPE), and the modified electrode was used for electrochemical detection of  $\rho$ -NP in 0.1 M acetate buffer at pH 4.5. The modified electrode exhibited high sensitivity, stability, reproducibility, and a low limit of detection under the optimum conditions.

## Experimental work

### Chemicals and equipment

Fe(NO<sub>3</sub>)<sub>3</sub>·9H<sub>2</sub>O (BDH), HAuCl<sub>4</sub> and  $\rho$ -NP (Boss Chemical Industry Co., Ltd., China). Acetate buffer solution (ActB) at pH 4.5 was used as the supporting electrolyte. All solutions were prepared with distilled water, and the investigations were run at room temperature ( $25 \pm 0.5$  °C). The chemical reagents utilized in this study were analytical grade and were used without further purification. All electrochemical investigations were carried out on a Biologic signal channel SP-200 with EC-lap software equipped with a typical three-electrode electrochemical cell that involved Ag/AgCl as the reference electrode, Pt wire as an auxiliary electrode, and CPE as the working electrode (3 mm inside diameter). The pH of the solution was monitored using an OHAUS starter 3100 pH

meter. Fourier transform infrared (FTIR) spectroscopy was performed on a Perkin Elmer (Spectrum 100, FT-IR spectrometer) as a KBr compact pellet in the wavenumber range of 4000 to 500  $\text{cm}^{-1}$ . UV–vis spectra were obtained using a 1650 SAM ADEM spectrophotometer in the wavelength range of 300–800 nm. High-resolution transmission electron microscopy (HR-TEM imaging) was performed on a TEM-JEM 1011 scanning electron microscope, and energy-dispersive X-ray spectroscopy (EDS) was carried out using a Jeol-760 FE-SEM. X-ray diffraction (XRD) was performed with a Rigaku D Imax VBIPC 2550 X-ray diffractometer at diffraction angles ranging from 10 to 110° with Co  $\text{K}\alpha$  radiation ( $\lambda = \text{Å}$ ).

### AuNPs, $\text{Fe}_3\text{O}_4$ NPs, and Au- $\text{Fe}_3\text{O}_4$ nanocomposite preparation

The *Hyssopus officinalis*-L extract was prepared by boiling 20 g of dry flower with 250 ml of distilled water in a sealed vessel for one hour in a steam bath. The liquid was allowed to reach a steady-state overnight, after which the solution was filtered, the filtrate solution was dried in an oven at 80 °C for 48 h, and then the powder was collected and dissolved in distilled water to prepare the stock solution at 400 ppm. The preparation of AuNPs and  $\text{Fe}_3\text{O}_4$ NPs was performed by adding 1 ml of extract to 9 ml of 1 mM  $\text{HAuCl}_4$  and 10 mM  $\text{Fe}(\text{NO}_3)_3 \cdot 9\text{H}_2\text{O}$  stock solutions, respectively. The color of the solution turns dark violated and dark brown (after gentle heating), which indicates the formation of AuNPs and  $\text{Fe}_3\text{O}_4$ NPs, respectively.

For Au- $\text{Fe}_3\text{O}_4$  nanocomposite synthesis, 2 ml of extract solution was mixed with 9 ml of each stock solution; in this case, the solution color changed after gentle heating from olive color to brown color. The change in color for AuNPs,  $\text{Fe}_3\text{O}_4$ NPs, and Au- $\text{Fe}_3\text{O}_4$  nanocomposite is depicted in Fig. 1 After two days the nanosolution was centrifuged for 15 mins at 4500 rpm, the liquid was decanted, while the solid part was retained for future use.

### Preparation of modified carbon paste electrode

The modified CPE was prepared by mixing 70% graphite with 30% paraffin oil to form a homogenous paste. The paste was inserted into the electrode cavity, and the surface was smoothed using clean filter paper. The electrochemical activity of the prepared nanoparticles was tested after casting 10  $\mu\text{L}$  of the nanosolution over the electrode surface and allowed to dry at room temperature. It is worth mentioning that 5  $\mu\text{L}$  of 5% Nafion suspension in ethanol was dropped to increase the binding strength and conductivity of the electrode.

### Electrochemical activity analysis

Cyclic voltammetry (CV) and electrochemical impedance spectroscopy (EIS) were employed to study the electrochemical activity at the various modified electrodes in 1 mM  $\text{K}_3[\text{Fe}(\text{CN})_6]$  mixed with 0.1 M KCl solution without  $\rho$ -NP. CV was performed in the potential range at -0.2 to 0.8 V versus Ag/AgCl, while EIS was tested in the frequency range of 100 kHz to 1 Hz at 235 mV versus Ag/AgCl with a 10 mV amplitude. Square wave Puls voltammetry (SWPV) was applied in acetate buffer solution with a specific concentration of  $\rho$ -NP in the potential range of -0.9 V to +1.0 V versus Ag/AgCl with a step high of 5 mV plus a height of 75 mV and a plus width of 10 ms.

## Results and discussion

### Characterization

#### FTIR and UV–vis spectra

FTIR analysis was carried out to identify the main functional group in the *Hyssopus officinalis*-L extract, which is responsible for the formation of the nanoparticles in the range of

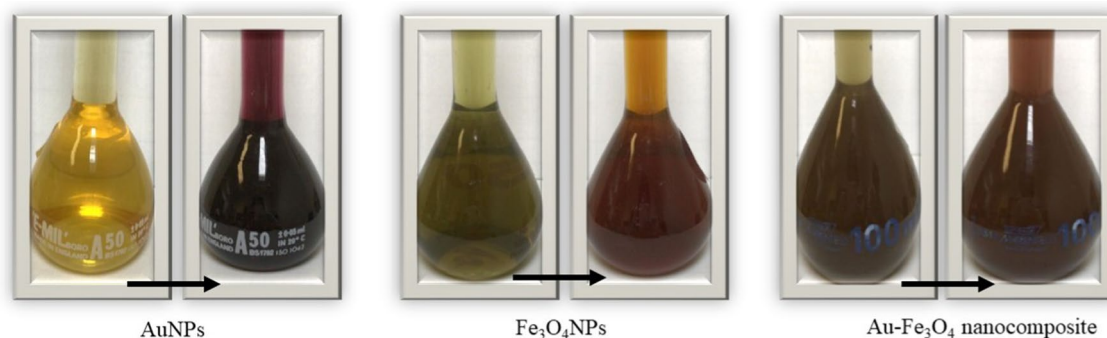


**Fig. 1** The change in color for AuNPs,  $\text{Fe}_3\text{O}_4$ NPs, and Au- $\text{Fe}_3\text{O}_4$  nanocomposites

4000–500  $\text{cm}^{-1}$ . The measurement was performed on the dry powder of each material mixed with KBr and pelletized.

FTIR spectra were measured for Hyssopus Officinalis-L extracts (Fig. 2A(a)), Au-Fe<sub>3</sub>O<sub>4</sub> nanocomposite (Fig. 2A(b)), Fe<sub>3</sub>O<sub>4</sub>NPs (Fig. 2A(c)) and AuNPs (Fig. 2A(d)). The spectra of Hyssopus Officinalis-L extract reflect a broad band at 3394  $\text{cm}^{-1}$  raised from the Str O–H bond, and the weak band at 2935  $\text{cm}^{-1}$  is attributed to the Str C–H bond. Moreover, the bands that appeared at 1703  $\text{cm}^{-1}$  and 1610  $\text{cm}^{-1}$  were due to Str C=O and C=C aromatics, respectively, the band at 1398  $\text{cm}^{-1}$  reflected bending O–H, while the band at 1264  $\text{cm}^{-1}$  represented Str C–O. The band at 1089  $\text{cm}^{-1}$  was produced from Str C–C.

On the other hand, the FTIR spectra of AuNPs, Fe<sub>3</sub>O<sub>4</sub>NPs, and Au-Fe<sub>3</sub>O<sub>4</sub> nanocomposites show a relative shift of bands with decreasing intensity. As a deduction, the main components in Hyssopus officinalis-L extracts, such as phenylacetaldehyde, isopinocampone, myrtenol, and pino-camphonethat (Kotyuk 2015), which contain O–H, C=O, and C=C groups, could be accountable for the formation of the nanomaterials and confirm that Hyssopus officinalis-L extract works as a reducing and capping agent (Rodríguez-León et al. 2019)(Erkan et al. 2014).

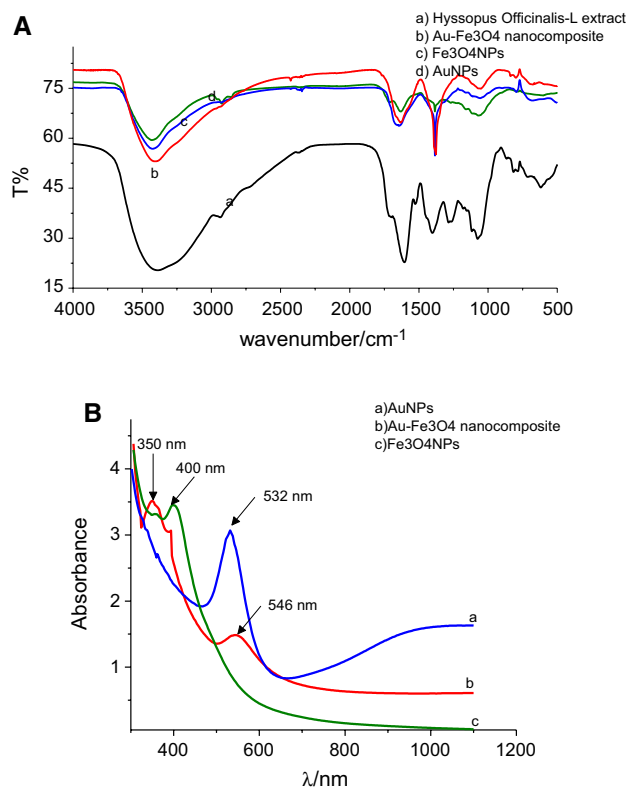


**Fig. 2** (A) FTIR spectra of a) Hyssopus officinalis-L, b) Au-Fe<sub>3</sub>O<sub>4</sub> nanocomposite c) Fe<sub>3</sub>O<sub>4</sub>NPs, and d) AuNPs, and (B) UV-vis absorbance of a) AuNPs, b) Au-Fe<sub>3</sub>O<sub>4</sub> nanocomposite and c) Fe<sub>3</sub>O<sub>4</sub>NPs,

The formation of AuNPs, Fe<sub>3</sub>O<sub>4</sub>NPs, and Au-Fe<sub>3</sub>O<sub>4</sub> nanocomposites was established using UV-vis spectra, as shown in (Fig. 2B(a-c)). Figure 2B(a) represents AuNPs with a sharp peak at 532 nm, and AuNPs exhibited localized surface plasmon resonance (LSPR) in the visible region between 500 and 600 nm due to the collective oscillation of electrons in the conductive band. As described, AuNPs formed through three steps: a nucleation step followed by an aggregation step and reduction as the final step to form spherical particles (Jim-Yang Lee 2012). The UV-vis absorption spectra confirm the formation of Fe<sub>3</sub>O<sub>4</sub>NPs and reflect the peak at 400 nm due to LSPR, which indicates the conversion of Fe(NO<sub>3</sub>)<sub>3</sub>·9H<sub>2</sub>O to Fe<sub>3</sub>O<sub>4</sub>NPs, as denoted in Fig. 2B(c). As suggested, the Fe<sub>3</sub>O<sub>4</sub>NPs that were synthesized using the bioreduction method exhibited UV-vis peaks in the range of 400 nm-600 nm (Rosli et al. 2018); this result is compatible with different investigations reported by other researchers (Rosli et al. 2018; Mahdavi et al. 2013; Saif et al. 2019). The UV-vis spectra of a mixture of Au-Fe<sub>3</sub>O<sub>4</sub> nanocomposites (Fig. 2B(b)) reflect a redshift in the peak of AuNPs and a blueshift of the Fe<sub>3</sub>O<sub>4</sub>NP peak when compared to the spectra of an individual component. The shift of the peak position confirms the coupling of bimetallic nanoparticles. This result may explain the difference in the dielectric environment around the nanoparticles since the Fe<sub>3</sub>O<sub>4</sub>NPs dielectric constant around AuNPs is higher than the air around AuNPs (Shan and Zhang 2018).

### SEM, EDS, and HR-TEM imaging

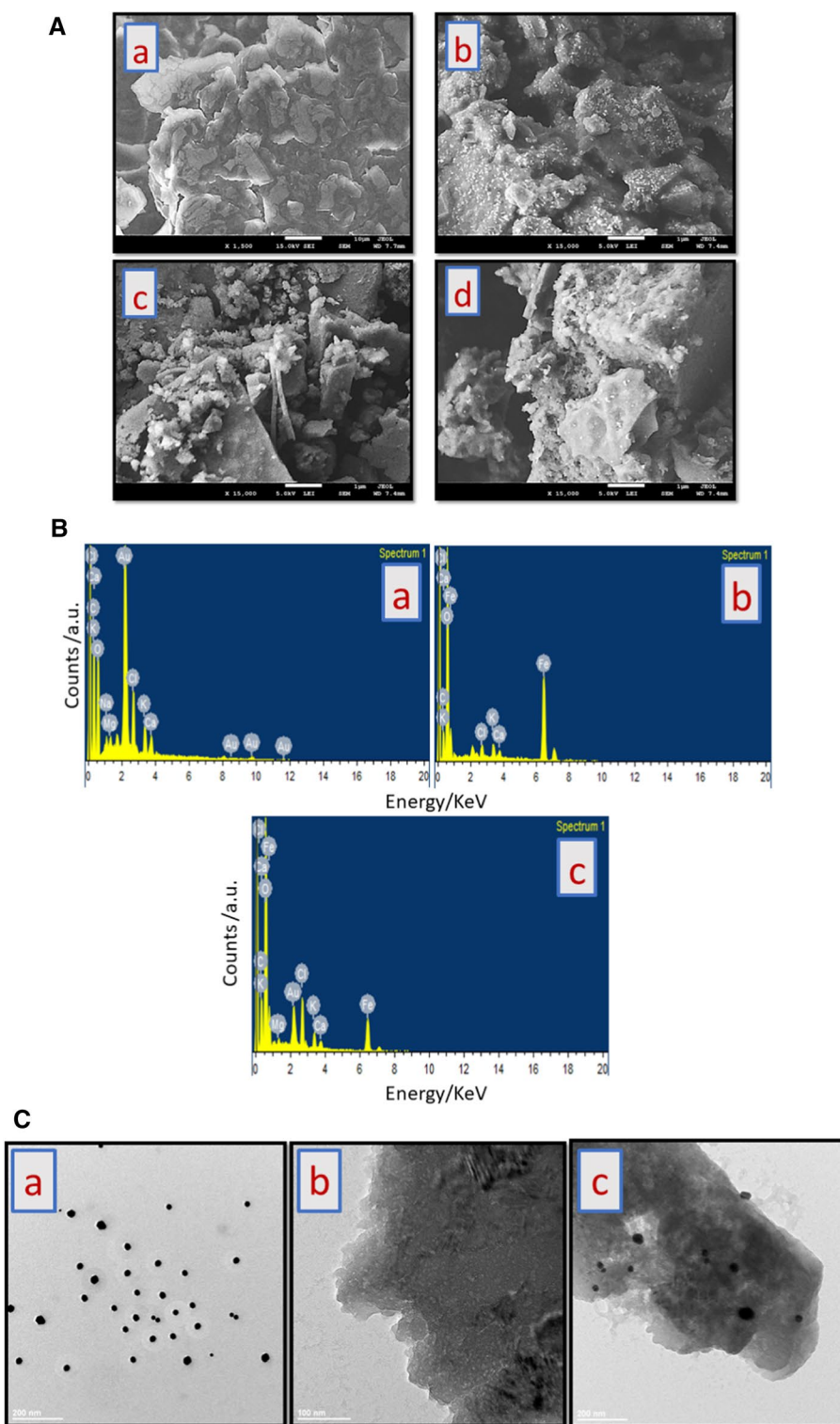
Scanning electron microscopy is a procedure used for the characterization and visualization of sample surfaces. This method is completely capable of monitoring the size, distribution of particles, and morphology of samples at the micro- and nanoscales (Mansoureh and Parisa 2018).

The surface morphology of the CPE electrode (Fig. 3A(a)) reflects overlay flakes of graphite with a flat surface. The SEM image in Fig. 3A(b) shows that biosynthesized AuNPs are condensed distributed and round spherical shaped, and no aggregation has appeared, which suggests that Hyssopus officinalis-L provides an excellent stabilizing and capping agent for AuNP formation. The prepared Fe<sub>3</sub>O<sub>4</sub>NPs (Fig. 3A(c)) show two shapes, puffy aggregated particles and large and bulk cuboidal particles. Aggregation of the Fe<sub>3</sub>O<sub>4</sub>NPs is expected due to their magnetic properties (Yadav et al. 2020). Similar results were reported by others (Yadav et al. 2020)(Ghanbari et al. 2014)(Devatha et al. 2018)(Mareedu et al. 2021).

However, the SEM image of the Au-Fe<sub>3</sub>O<sub>4</sub> (Fig. 3A(d)) nanocomposite reflected the coupling between AuNPs and Fe<sub>3</sub>O<sub>4</sub>NPs.

The elemental composition was examined using energy-dispersive spectroscopy (EDS) for individual AuNPs,

**Fig. 3** (A) SEM of a) CPE b) AuNPs, c)  $\text{Fe}_3\text{O}_4$ NPs, and d) Au- $\text{Fe}_3\text{O}_4$  nanocomposite, (B) EDS of a) AuNPs, b)  $\text{Fe}_3\text{O}_4$ NPs, and c) Au- $\text{Fe}_3\text{O}_4$  nanocomposite and HR-TEM image of a) AuNPs, b)  $\text{Fe}_3\text{O}_4$ NPs, and c) Au- $\text{Fe}_3\text{O}_4$  nanocomposite



$\text{Fe}_3\text{O}_4$ NPs, and Au- $\text{Fe}_3\text{O}_4$  nanocomposites, as depicted in Fig. 3B(a-c). The signal of the Au- $\text{Fe}_3\text{O}_4$  nanocomposite confirms the coupling of these particles, and the analysis of the spectra in Fig. 3B (a and b) confirms the presence and formation of AuNPs and  $\text{Fe}_3\text{O}_4$ NPs. Another chemical

element presents one EDS spectrum arising from *Hyssopus officinalis*-L extract that surrounds the nanoparticles (Rodríguez-León et al. 2019). However, the weight percentages of Au and Fe in the Au- $\text{Fe}_3\text{O}_4$  nanocomposite are 7.74% and 16.50% (w/w%), respectively, compared with 32.74%

of Au and 47.54% of Fe for the individual nanosolutions. The diminishing weight percentage is a good indication of coupling and formation of the Au-Fe<sub>3</sub>O<sub>4</sub> nanocomposite.

HR-TEM imaging analysis is a helpful tool to investigate nanoscale properties of the size, distribution, and morphology of particles and crystalline materials. The analysis was performed by applying a drop of nanoparticle solution on a TEM copper grid coated with carbon. The film was dried for 30 min, and TEM images were obtained from the different counts for AuNP, Fe<sub>3</sub>O<sub>4</sub>NP, and Au-Fe<sub>3</sub>O<sub>4</sub> nanocomposite samples, as represented in Fig. 3C(a-c). Analyzing the TEM image of AuNPs (Fig. 3C(a)) shows that particles are mostly spherical with a slight heterogeneity of shape and size. The particles were well distributed with the *Hyssopus Officinalis-L* extract matrix, which is good evidence that *Hyssopus Officinalis-L* serves as a capping agent to insulate AuNPs and prevent the aggregation process.

Fe<sub>3</sub>O<sub>4</sub>NPs (Fig. 3C(b)) exhibit high accumulation, as the particles imply overlap and show a dense black area, and the agglomeration trend is ascribed to the magnetic properties of Fe<sub>3</sub>O<sub>4</sub>NPs, as reported elsewhere ((Adyani and Soleimani 2019; Nasrollahzadeh and Sajadi 2016)). Figure 3C(c) reflects the formation of the Au-Fe<sub>3</sub>O<sub>4</sub> nanocomposite. The dark spherical particles represent AuNPs with high electron density, whereas the light area is associated with Fe<sub>3</sub>O<sub>4</sub>NPs with lower electron density (Oliveira-Filho et al. 2021).

X-ray diffraction (XRD) was performed to confirm the formation of the Au-Fe<sub>3</sub>O<sub>4</sub> nanocomposite and the change in the crystal structure of AuNPs due to the incorporation of Fe<sub>3</sub>O<sub>4</sub>NPs.

**Figure 4a** shows the XRD of Fe<sub>3</sub>O<sub>4</sub>NPs, as described before. The low distinctive pattern is a strong indication of the amorphous nature of Fe<sub>3</sub>O<sub>4</sub>NPs, and the broad peak arises from the carbon-containing biomolecule from **Hyssopus Officinalis-L extract**. A similar XRD pattern for the bioreduction preparation of Fe<sub>3</sub>O<sub>4</sub>NPs was obtained (((Luo et al. 2014; Wang 2013; Mohan Kumar et al. 2013; Mareedu et al. 2021))). Fe<sub>3</sub>O<sub>4</sub>NP weak peaks were centered at approximately 2θ of 34.0° and 63.8°, which correspond to (101) and (521), respectively, indicating the magnetite phase of iron.

oxide (Predescu et al. 2018). The examined diffraction pattern was fitted with the standard XRD peaks of Fe<sub>3</sub>O<sub>4</sub>NPs with JCPDS file no: 00–003–0863 and proved the creation of magnetite phases. The XRD data are in agreement with the data reported previously (((Yew et al. 2020; Basavegowda et al. 2014; Yadav et al. 2020))).

AuNPs (Fig. 4b) reflect the plane phase, as (111), (200), (220), and (222) show a significant crystallinity phase of AuNPs, confirming the structure of AuNPs to face center cubic (fcc). The crystallinity of AuNPs is pure by comparing their XRD pattern with the database JCPDS file no: 00–004–0784 (Anuradha et al. 2015).

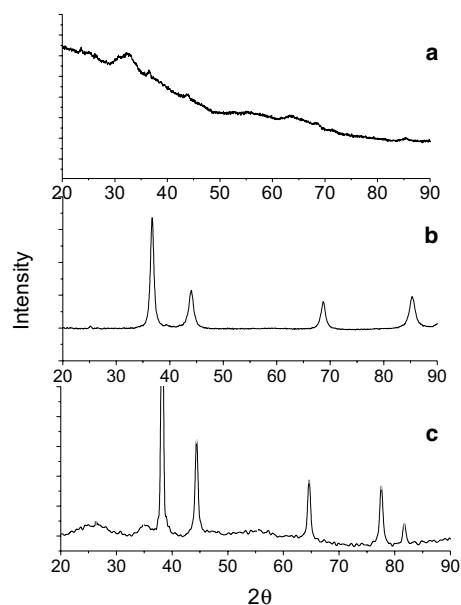


**Fig. 4** XRD spectra of a) Fe<sub>3</sub>O<sub>4</sub>NPs, b) AuNPs, and c) Au-Fe<sub>3</sub>O<sub>4</sub> nanocomposite

The crystalline structure and the phase identification of the Au-Fe<sub>3</sub>O<sub>4</sub> nanocomposite are shown in Fig. 4c. A careful examination of the XRD pattern revealed a shift in the peak position of AuNPs and Fe<sub>3</sub>O<sub>4</sub>NPs, and the slight peak shift of the 2θ value was strong evidence of the formation of the Au-Fe<sub>3</sub>O<sub>4</sub> nanocomposite. A similar result was reported previously (Sheikh et al. 2018).

## Electrochemical investigation

The electrochemical test of different types of electrodes donated as bare CPE, CPE/AuNPs, CPE/Fe<sub>3</sub>O<sub>4</sub>NPs, and CPE/Au-Fe<sub>3</sub>O<sub>4</sub> nanocomposite electrodes was attempted by EIS and CV measurements in 1 mM K<sub>3</sub>[Fe(CN)<sub>6</sub>] mixed with 0.1 M KCl. As reported before, K<sub>3</sub>[Fe(CN)<sub>6</sub>] is considered a common probe electrolyte in surface science to characterize the modified electrode surface (Calam 2020). Figure 5A clarifies the EIS spectra as Nyquist plot for the bare and modified electrodes, the bare CPE electrode reflects the large, depressed semi-circle with diameter related to charging transfer resistance at the high-frequency region, which represents the controlling of the kinetics of electron transfer at probe | electrode interface, this behavior changes to small tail related to mass diffusion resistance at the low region. Conversely, all types of modified electrodes exhibited small semi-circle in the high-frequency region and long tails in the low-frequency region. The noticeable reduction in the semi-circle part of the modified electrode compared with the bare CPE electrode is strong evidence for enhancing conductivity, as shown in Table 1.

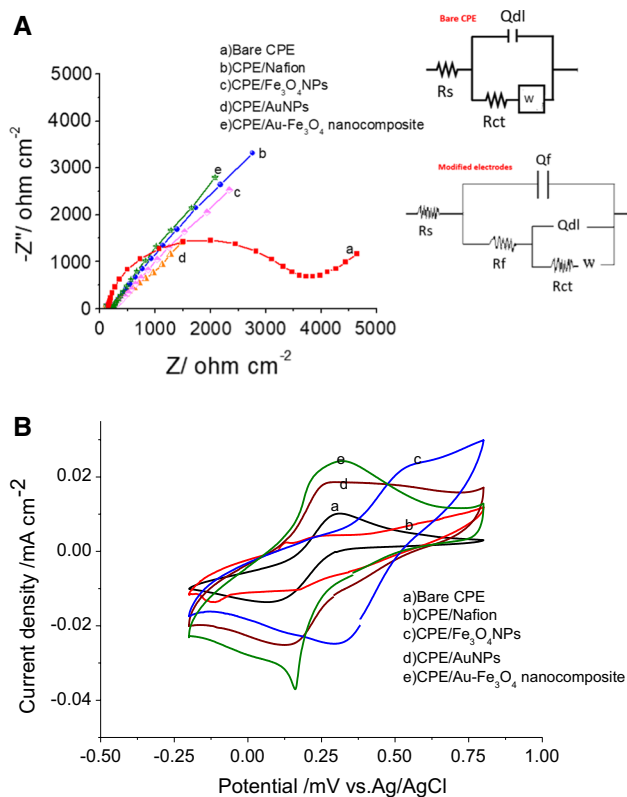


**Fig. 5** (A) Nyquist plots of EIS measurements and (B) cyclic voltammograms in 1 mM  $K_3[Fe(CN)_6]$  solution containing 0.1 mol/L KCl

**Table 1** Charge transfer resistance was found from the fitting method

Electrode	$R_{ct}/\Omega\text{ cm}^2$
CPE	5856
CPE/Nafion	162.9
CPE/AuNPs	177.8
CPE/ $Fe_3O_4$ NPs	202.7
CPE/Au- $Fe_3O_4$ nanocomposite	145.3

Zsim software was used to find the best fit equivalent circuit and to estimate the value of charge transfer resistance ( $R_{ct}$ ), according to  $R_s(Q_{dl}(R_{ct}W))$  for the bare CPE electrode and  $R_s(Q_f(R_f(Q_{dl}(R_{ct}W))))$  for the other modified electrodes. The circuit involved the solution resistance ( $R_s$ ), charge transfer resistance ( $R_{ct}$ ), film resistance ( $R_f$ ), Warbag resistance ( $W$ ), ( $Q_f$ ) and ( $Q_{ct}$ ) as constant phase elements for the film and electrical double layer, respectively.

The rate constant  $k^o$  for charge transfer can be calculated according to Eq. 1 (Calam 2020), where  $R$  is the gas constant  $J/k.mol$ ,  $T$  is the absolute temperature ( $298\text{ }^\circ k$ ),  $n$  is the number of transferred electrons (one electron),  $F$  is the Faraday constant ( $96,485\text{ C/mol}$ ),  $A$  is the electrode surface area, and  $C$  is the  $K_3[Fe(CN)_6]$  concentration (1 mM)

$$k^o = \frac{RT}{R_{ct}n^2F^2AC}$$

The calculated rate constant was found to be  $13 \times 10^{-3}$  for the CPE/Au- $Fe_3O_4$  nanocomposite electrode compared to  $30 \times 10^{-5}$  for bare CPE, which proved the fast electron transfer on the CPE/Au- $Fe_3O_4$  nanocomposite electrode.

For further declaration of the bare CPE electrode and modified electrodes, the CV measurement was implemented in the potential range of -0.5 to 1.0 V versus Ag/AgCl, as shown in Fig. 5B, the figure exposed well-defined reversible redox peaks, which prove the transfer of one electron through the redox process of  $Fe^{+3}$  ions between the electrode and probe solution. In addition, the CV of CPE/Nafion was a measure for elucidation of whether the increased conductivity was due to pure Nafion, and it is clear that pure Nafion did not show an appreciable rise in redox peaks. The noteworthy CPE/Au- $Fe_3O_4$  nanocomposite electrode implies the highest redox peaks among all electrodes, which emphasizes the increase in the electrochemical activity of the nanocomposite. The oxidation current value for the CPE/Au- $Fe_3O_4$  nanocomposite electrode is  $0.024\text{ mAcm}^{-2}$ , compared to  $0.018\text{ mAcm}^{-2}$  (CPE/AuNPs),  $0.021\text{ mAcm}^{-2}$  (CPE/ $Fe_3O_4$ NPs) and  $0.010\text{ mAcm}^{-2}$  (bare CPE). This phenomenon was attributed to the fact that enlarging the surface area of the nanocomposite increased the number of active sites on the electrode surface and facilitated electron transfer at the electrode–electrolyte interface. The CPE/AuNPs and CPE/ $Fe_3O_4$ NPs presented lower responses regarding  $K_3[Fe(CN)_6]$  prob compared to the CPE/Au- $Fe_3O_4$  nanocomposite electrode.

### Optimization of electrochemical parameters

The electrochemical determination of  $\rho$ -NP was achieved by applying the SWPV technique under different conditions to optimize the best parameters in this study. These parameters include the type of supporting electrolyte, changing pH, accumulation time, scan rate, amount of Au- $Fe_3O_4$  nanocomposite added, and amount of Nafion added.

### Effects of supporting electrolyte

The effect of different types of buffer solutions at pH 4.5, including phosphate buffer (PhB) solution, Britton–Robinson buffer (BRB) solution, and acetate buffer (ActB) solution, in the electrooxidation of  $10\text{ }\mu\text{M}$   $\rho$ -NP was tested. The concentration of buffer solution was 0.1 M, as displayed in Fig. 6. The figure shows that the three types of buffers exhibited a current response signal, although the ActB solution shows the best current signal. Thus, 0.1 M ActB solution was chosen as the optimum electrolyte. The electrochemical activity of  $10\text{ }\mu\text{M}$   $\rho$ -NP in 0.1 M ActB pH 4.5 on a CPE/

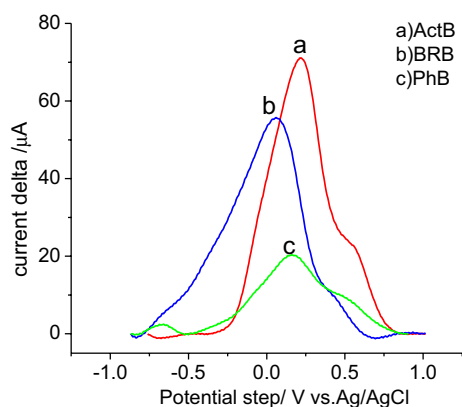


**Fig. 6** SWV curves of 10  $\mu\text{M}$   $\rho\text{-NP}$  in different buffer solutions at pH 4.5

$\text{Au-Fe}_3\text{O}_4$  nanocomposite electrode was investigated using SWPV in a potential range of -0.9 to 1.0 SWPV, as presented in Fig. 6, the spectra reflected the oxidation peak at 0.21 V versus Ag/AgCl. The potential in the oxidation region is lower than that reported previously, but is consistent with others (V. de A. Pedrosa 2003; Garbellini et al. 2007; Jiang et al. 2010; Zhao et al. 2007). As reported, the reduction of  $\rho\text{-NP}$  to p-hydroxyaminophenol at -0.79 V through the transfer of four electrons and four protons, whereas the oxidation of  $\rho\text{-NP}$  into nitrosophenol through two electrons and two proton transfers at a potential of 0.21 V (Karupiah et al. 2014; Arulraj et al. 2015). However, in this study, the modification of the CPE electrode affects the oxidation process of  $\rho\text{-NP}$  rather than its reduction. The redox mechanism can be represented in Eqs. 1 and 2:

### Effect of pH

The influence of the changing pH of the ActB solution on the electrochemical oxidation of 10  $\mu\text{M}$   $\rho\text{-NP}$  was investigated in the range of 3.5–8.5, as presented in Fig. 7A. Clearly, the current response increases from 3.5 to 4.5 and then gradually decreases with increasing pH. Accordingly, a pH of 4.5 was selected as the optimum value for the next measurement. It is interesting to note the maximum current response at pH 4.5, which is lower than the  $\text{pK}_a$  value of  $\rho\text{-NP}$  ( $\text{pK}_a = 7.16$ ) (Yin et al. 2012; Anslyn and Dougherty 2006), which means that  $\rho\text{-NP}$  adsorbed on the CPE/ $\text{Au-Fe}_3\text{O}_4$  nanocomposite electrode in a nondissociated form. Referring to an earlier report, the non-dissociated form of  $\rho\text{-NP}$  is hydrophobically compared to the dissociated form (ionic form), so the interaction between the CPE/ $\text{Au-Fe}_3\text{O}_4$  nanocomposite electrode and  $\rho\text{-NP}$  needs to be higher than the hydrophobic force (Arulraj et al. 2015). Figure 7B shows the change in peak potential with pH value, the potential shift to a more negative value with increasing the pH of the solution, which emphasizes

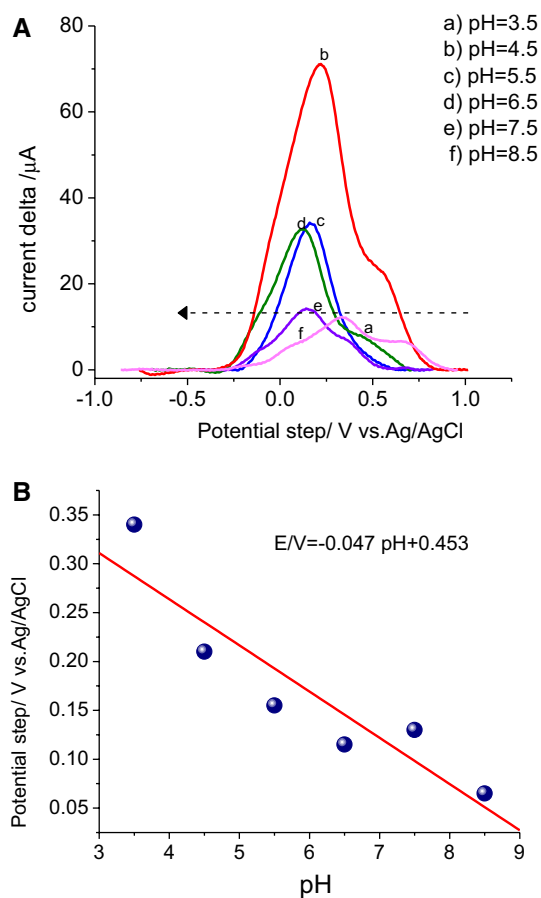


**Figure 7** (A) SWPV curves of 10  $\mu\text{M}$   $\rho\text{-NP}$  in 0.1 M acetate buffer (A) at different pH values and (B) changes in the potential for oxidation peaks with pH

the involvement of protons in the oxidation process of  $\rho\text{-NP}$ . The linear equation of  $E/V = -0.047 \text{ pH} + 0.453$  with slope = 47 mV suggests that two electrons and two protons are required in the oxidation of  $\rho\text{-NP}$  on the CPE/ $\text{Au-Fe}_3\text{O}_4$  nanocomposite electrode surface, as shown above (Eq. 2).

### Effect of accumulation time

The influence of accumulation time on the electrooxidation of 10  $\mu\text{M}$   $\rho\text{-NP}$  on the CPE/ $\text{Au-Fe}_3\text{O}_4$  nanocomposite electrode was monitored and recorded in Fig. 8 in 0.1 M ActB solution at pH = 4.5. The figure reflects that the oxidation current response increases from direct immersion time to five minutes, after which the signal gradually decreases with increasing immersion time. This situation suggests that the adsorption of  $\rho\text{-NP}$  increases from 0 min to five minutes, the decrease in current above five minutes detects the saturation of  $\rho\text{-NP}$  on the electrode surface, and there is no more accessible site on the surface. Therefore, to increase the work sensitivity and productivity, the optimal five minutes were applied for further measurement.



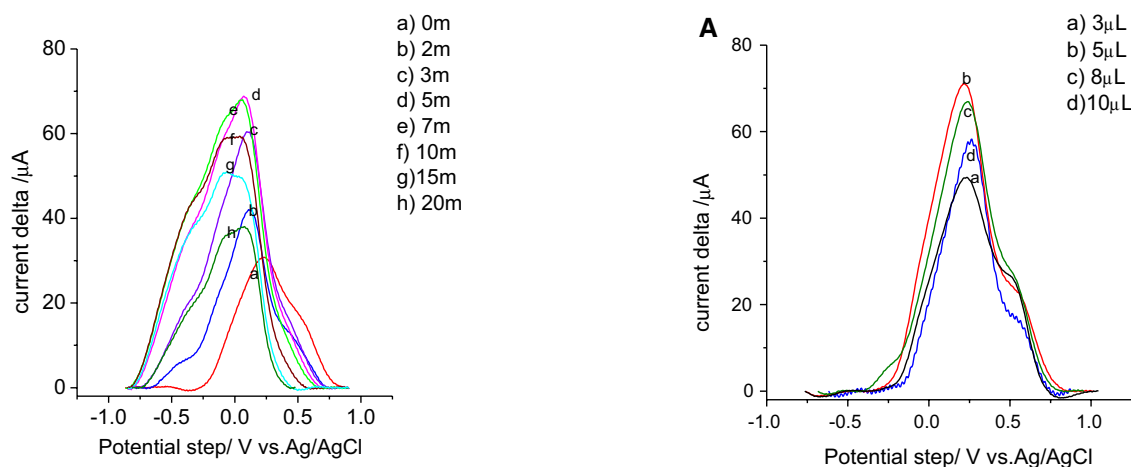


**Fig. 8** Effect of the accumulation time on the SWPV of the CPE/Au-Fe<sub>3</sub>O<sub>4</sub> nanocomposite electrode in the presence of 10 μM ρ-NP in 0.1 M ActB solution at pH 4.5

### Effect of loading amount of Nafion and Au-Fe<sub>3</sub>O<sub>4</sub> nanocomposite

The thicknesses of the Nafion (3, 5, 8, and 10 μL) and Au-Fe<sub>3</sub>O<sub>4</sub> nanocomposite (3, 5, 8, and 10 μL) films are considered the critical factors controlling the oxidation current response, as shown in Fig. 9 A and Fig. 9B, respectively. An ascending increase in the current signal with an increase in the loading amount of the Au-Fe<sub>3</sub>O<sub>4</sub> nanocomposite from 3 μL to 10 μL, while the current signal increases when the thickness of the Nafion layer increases from 3 μL to 5 μL. Further loading of Nafion (8 μL and 10 μL) caused a reduction in the sharpness of the oxidation current signal. This decrease in the current response was mostly resent to increasing the thickness of the Nafion layer, which hindered electron transfer between the ρ-NP and CPE/Au-Fe<sub>3</sub>O<sub>4</sub> nanocomposites at the electrode surface. The optimum quantity of the Nafion layer provides good stability of the modification on the electrode surface (Sacara et al. 2017). Therefore, 5 μL of Nafion layer and 10 μL of Au-Fe<sub>3</sub>O<sub>4</sub> nanocomposite loading amount were preferred as the optimum amount for further experiments.

### Effect of scan rate

CV measurements were used to investigate the effect of a change in scan rate on the oxidation current of 10 μM ρ-NP presented in Fig. 10A. It was found that an increase in the scan rate from 50 to 500 mV caused a slight increase in the oxidation current signal and a shift in the oxidation potential to a more positive value. A similar result was reported in a previous study of the effect of change scan rate of glucose oxidase modified graphite rod (GOx/

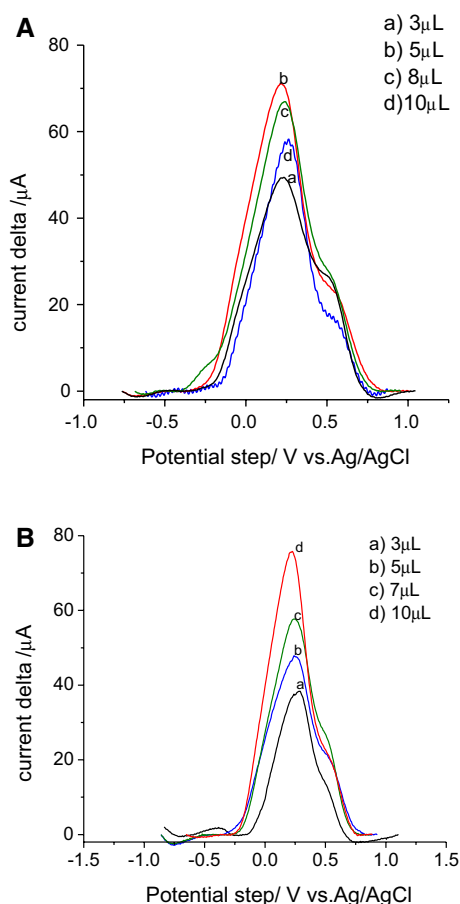


**Fig. 9** Effect of loading amount of (A) Nafion, and (B) Au-Fe<sub>3</sub>O<sub>4</sub> nanocomposite on the SWPV of CPE/Au-Fe<sub>3</sub>O<sub>4</sub> nanocomposite electrode in the presence of 10 μM ρ-NP in 0.1 M ActB solution at pH 4.5

GR) and AuNPs and GOx modified graphite rod (GOx/AuNPs/GR) electrode (Ramanavicius et al. 2017). Notably, a linear relationship correlates the oxidation current response with the square root of the scan rate, as displayed in Fig. 10B, which presupposes that the oxidation process of ρ-NP on the CPE/Au-Fe<sub>3</sub>O<sub>4</sub> nanocomposite electrode is under the diffusion-controlled mechanism. The plot of log oxidation peak currents versus log scan rate, i.e.,  $\log i \text{ (mA)} = 0.276 \log \nu \text{ (mVs}^{-1}\text{)} - 1.26$  with  $R^2$  of 0.991 (Fig. 10 (C)), revealed a slope of 0.276 mV, verifying that the reaction was under a diffusion-controlled process. It was reported that the linear relationship produces from plotting log I versus log  $\nu$  with slope of 0.5 for pure diffusion process and slope of 1.0 for pure adsorption process, the slope value between 0.5 and 1.0 corresponds to process under diffusional/ adsorption control (L.M. Gonçalves et al 2010). In this study, the slope is 0.276 which confirms that the reaction is under diffusion control.

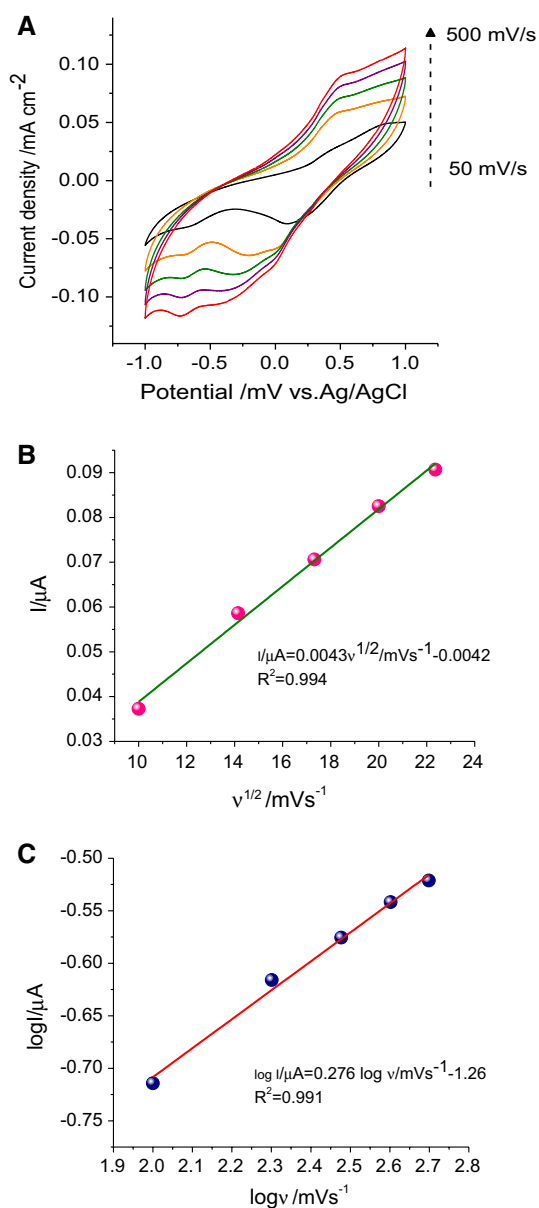


**Fig. 10** Effect of change in (A) scan rate on the CV of CPE/Au-Fe<sub>3</sub>O<sub>4</sub> nanocomposite electrode in the presence of 10 μM ρ-NP, (B) current vs.  $\nu^{1/2}$  and (C) log current vs.  $\log \nu$  in 0.1 M ActB solution at pH 4.5

#### Calibration curve of different concentrations of ρ-NP.

Figure 11A shows the effect of successive addition of (3–50 μM) of ρ-NP on the SWPV response to 0.1 M ActB solution at pH 4.5 at room temperature under the optimum conditions described above. The SWPV spectra demonstrate an appreciable increase in the oxidation current response as a result of the gradual addition of ρ-NP. The calibration plot in Fig. 11B displays a linear relationship between the ρ-NP concentration and current signal. The fitting Equation  $I(\mu\text{A}) = 9.137C(\mu\text{M}) + 2.363$  describes the linear correction

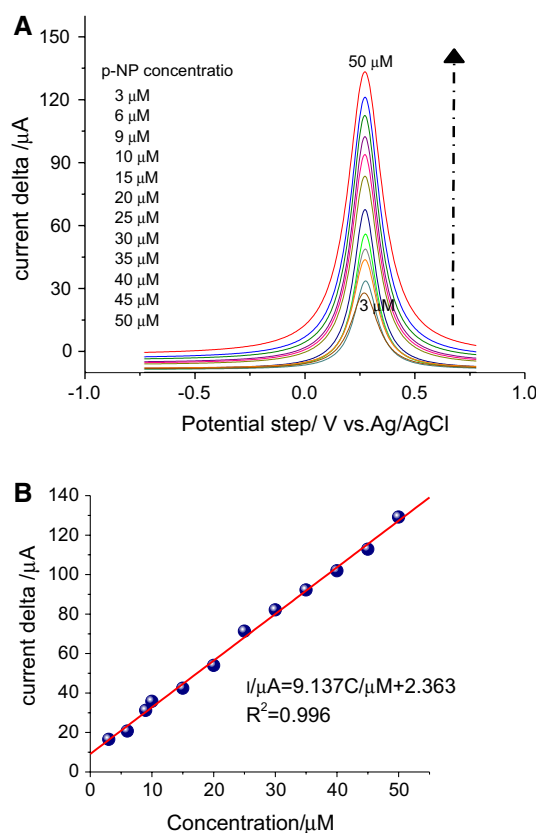


**Fig. 11** Effect of change of ρ-NP concentration on (A) SWPV and (B) oxidation current signal of CPE/Au-Fe<sub>3</sub>O<sub>4</sub> nanocomposite electrode in 0.1 M ActB solution at pH 4.5

with  $R^2 = 0.996$ . The limit of detection (LOD = 0.023 μM) and limit of quantification (LOQ = 0.079 μM) were calculated from 3\*standard error of three measurements of blank buffer/slope from the calibration curve and 10\*standard error of three measurements of blank buffer/slope from the calibration curve, respectively. On the other hand, the sensitivity of the modified electrode is considered a crucial factor of the designed sensor. For this reason, the sensitivity of the CPE/Au-Fe<sub>3</sub>O<sub>4</sub> nanocomposite electrode was calculated based on the slope of the calibration plot according to the equation sensitivity = slope/area of the electrode (Khan et al. 2019). The sensitivity of the electrode was found to be 64.63 μA/μM cm<sup>2</sup>, where the CPE surface area was 0.1414 cm<sup>2</sup>. The comparison of the LOD of the CPE/Au-Fe<sub>3</sub>O<sub>4</sub> nanocomposite electrode as an electrochemical sensor for ρ-NP with the previously reported sensor is tabulated in Table 2 (Fig. 12).

#### Study of selectivity, stability, and reproducibility.

The effect of adding different concentrations of another phenol derivative to the oxidation current signal of 10 μM of ρ-NP was examined. The results show that

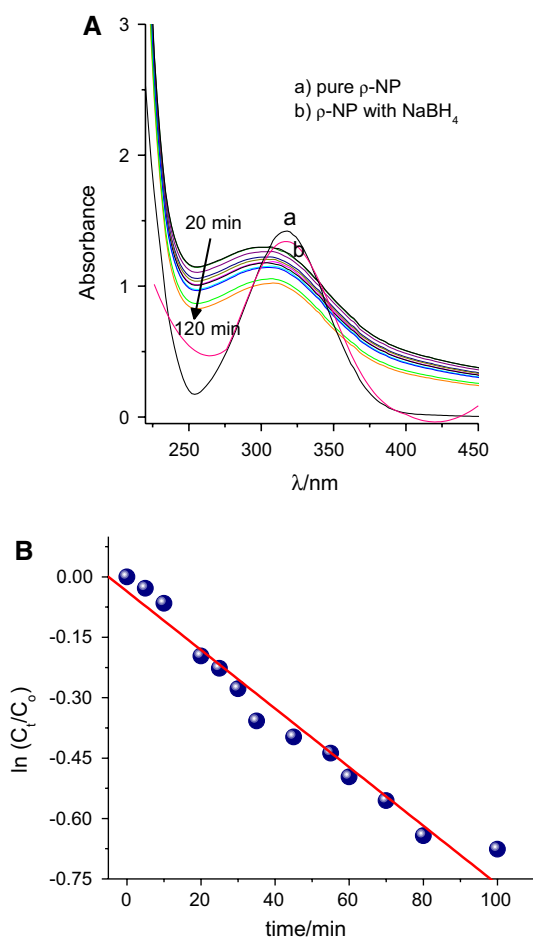


**Fig. 12** (A) UV–vis absorption spectra of a) pure  $\rho$ -NP, b)  $\rho$ -NP reduction by  $\text{NaBH}_4$  in the presence of  $\text{Au-Fe}_3\text{O}_4$  nanocomposite catalyst at different times, and (B) plot of  $\ln(C_t/C_0)$  versus time

foreign substances, such as 35-fold 2,4-dichlorophenol (RSD = 4.95), 20-fold 3-chlorophenol (RSD = 3.79), 20-fold 2-chlorophenol (RSD = 4.08), 35-fold 2-nitrophenol (RSD = 3.58) and 40-fold 4-amino phenol (RSD = 2.81), had no significant effect on the original current signal of  $\rho$ -NP. Based on the RSD of each interfering substance being less than 5%, the CPE/ $\text{Au-Fe}_3\text{O}_4$  nanocomposite electrode has

excellent selectivity for the target analyte. The reducibility of the CPE/ $\text{Au-Fe}_3\text{O}_4$  nanocomposite electrode was measured by the formulation of five different electrodes and the current response for 10  $\mu\text{M}$   $\rho$ -NP. The difference between the current values for the various electrodes, i.e., RSD, is 5.23%. Moreover, the stability of the prepared CPE/ $\text{Au-Fe}_3\text{O}_4$  nanocomposite electrode was evaluated using 20 consecutive cycles of 10  $\mu\text{M}$   $\rho$ -NP in 0.1 M ActB solution, and the detected RSD was 0.013%, suggesting excellent stability of the proposed electrode.

#### Evolution of $\rho$ -NP in real tap water and wastewater samples.

The ability to utilize CPE/ $\text{Au-Fe}_3\text{O}_4$  nanocomposite electrodes in a real sample, such as wastewater and tap water, was evaluated after filtration using Waterman filter paper by applying the standard addition method. The recovery calculation result of  $\rho$ -NP from each water sample was in the range of 96–112%, as summarized in Table 3. The achieved recovery results are a strong indication of the reliability and effectivity of the developed CPE/ $\text{Au-Fe}_3\text{O}_4$  nanocomposite electrode for sensing  $\rho$ -NP in real environments.

#### Study of the catalytic effect of the $\text{Au-Fe}_3\text{O}_4$ nanocomposite on $\rho$ -NP removal.

Regarding environmental protection, the removal of  $\rho$ -NP is required; thus, the effect of the catalytic activity of the  $\text{Au-Fe}_3\text{O}_4$  nanocomposite on the degradation of 30  $\mu\text{M}$   $\rho$ -NP with time was examined. As reported, the use of  $\text{NaBH}_4$  as a reduction agent and nanomaterial as catalysis is the most efficient reduction method  $\rho$ -NP (Salaheldin 2017). Langmuir–Hinshelwood described that the reduction of  $\rho$ -NP using  $\text{NaBH}_4$  can be classified into two types depending on the type of interaction of the nanocatalyst in the solution: first, a heterogeneous route since the catalyst is adsorbed on the  $\rho$ -NP surface and second, a homogeneous route in which the catalyst occurs by leached atoms from the  $\rho$ -NP surface (Wang et al. 2016).

**Table 2** Evaluation of  $\rho$ -NP using different electrochemical sensors

Modified electrode	Method	Linear range ( $\mu\text{M}$ )	LOD ( $\mu\text{M}$ )	Ref. No
CMO Ns	DPV	Up to 249	0.01	Balasubramanian et al. (2019)
GCE/ $(\text{Fe}_3\text{O}_4\text{-Pt})$ NPs	DPV	0.1–1.5	0.0337	Ramalingam et al. (2020)
GCE/rGO-180	DPV	50–800	42	Wiench et al. (2017)
LSCrRu0.075	SWV	25–500	7	Mojović et al. (2021)
GCE/AgNPs–chitosan	SWV	0.07–2.0	0.07	Lima et al. (2014)
GC/DB $\beta$ -CD-MWCNT	DPV	0.1–200	0.048	Yang et al. (2015)
GC/Ag-NPs	DPV	0.1–350	0.015	Karuppiah et al. (2014)
CPE/ $\text{Au-Fe}_3\text{O}_4$ nanocomposite	SWPV	0.3–50	0.023	This work

**Table 3** Recovery of  $\rho$ -NP in different water samples

Sample	Added [ $\mu$ M]	Found [ $\mu$ M]	Recovery [%]
Tap water	40	38.46	96.15
	45	45.44	100.98
	50	48.70	97.40
Wastewater	40	45.17	112.93
	45	46.16	102.58
	50	50.41	100.82

The degradation of 30  $\mu$ M  $\rho$ -NP in the presence of 1 ml  $\text{NaBH}_4$  (0.1 M) with and without 0.2 g/L  $\text{Au-Fe}_3\text{O}_4$  nanocomposites is shown in.

A shows that the  $\rho$ -NP degradation was enhanced with time, and the gradual decrease in the peak at 294 nm (after 20 min) indicates a decrease in the  $\rho$ -nitrophenolate ions from  $\rho$ -NP (Castañeda et al. 2016) and a peak shift from 322 nm (after 120 min) in the absence of the  $\text{Au-Fe}_3\text{O}_4$  nanocomposite to 302 nm in the presence of nanoparticles associated with the amino group of  $\rho$ -AP (aminophenol).

The rate constant  $K$  was calculated from equation

$$\ln\left(\frac{C_t}{C_o}\right) = k.t$$

where  $C_o$  and  $C_t$  represent the initial absorbance ( $A_o$ ) and absorbance after a period of time ( $A_t$ ) at  $\lambda_{\text{max}}$ . The linear relationship of plotting  $\ln(C_t/C_o)$  against time produces  $K$  equal to  $0.01 \text{ min}^{-1}$ , which indicates that the degradation of  $\rho$ -NP in the presence of  $\text{Au-Fe}_3\text{O}_4$  nanocomposite flows pseudofirst-order with a correlation coefficient  $R^2$  of 0.999 since the concentration of  $\text{NaBH}_4$  is excess compared with  $\rho$ -NP. The catalytic effect of the  $\text{Au-Fe}_3\text{O}_4$  nanocomposite on  $\rho$ -NP reduction may be due to the transfer of electrons at the  $\text{Au-Fe}_3\text{O}_4$  nanocomposite surface, which is affected by diffusion of  $\rho$ -NP molecules to or from the surface of the nanoparticles (Zhao et al. 2015) (Zayed and Eisa 2014).

## Conclusion

The  $\text{Au-Fe}_3\text{O}_4$  nanocomposite was successfully synthesized using *Hyssopus Officinalis*-L extract solution, and the fabricated nanocomposite was characterized by SEM, EDX, XRD, FTIR, UV–vis, and TEM. The ability of the CPE/ $\text{Au-Fe}_3\text{O}_4$  nanocomposite electrode to detect  $\rho$ -NP in ActB solution at pH 4.5 was evaluated. The  $\text{Au-Fe}_3\text{O}_4$  nanocomposite promote the electron transfer between the  $\rho$ -NP and electrode surface. The change in the potential sweep rate range of 50–500 mV/s indicates that the electrochemical reaction is under diffusion controlled. The electrochemical sensor exhibited LODs and LOQs of 0.023  $\mu$ M and 0.079

$\mu$ M, respectively, with high stability and reproducibility. Moreover, the  $\text{Au-Fe}_3\text{O}_4$  nanocomposite reflects remarkable catalytic activity toward removal of  $\rho$ -NP in the presence of  $\text{NaBH}_4$  as a reducing agent. Therefore, the  $\text{Au-Fe}_3\text{O}_4$  nanocomposite is considered an excellent nanomaterial for sensing and removing  $\rho$ -NP in a real environment. Future investigation should reflect the potential effects of  $\text{Au-Fe}_3\text{O}_4$  nanocomposite on electrochemical sensing of hazardous materials such as heavy metals or dyes.

## References

- Adyani SH, Soleimani E (2019) Green synthesis of  $\text{Ag/Fe}_3\text{O}_4/\text{RGO}$  nanocomposites by *Punica Granatum* peel extract: Catalytic activity for reduction of organic pollutants. *Int J Hydrogen Energy* 44:2711–2730. <https://doi.org/10.1016/j.ijhydene.2018.12.012>
- Anslyn E, Dougherty D, Modern physical organic chemistry, (2006) [https://books.google.com/books?hl=en&lr=&id=gY-Sxijk\\_tMC&oi=fnd&pg=PR23&ots=ewtFhcGmZh&sig=zq4DxAI4EDX-kMxwk7HaoZchR8E](https://books.google.com/books?hl=en&lr=&id=gY-Sxijk_tMC&oi=fnd&pg=PR23&ots=ewtFhcGmZh&sig=zq4DxAI4EDX-kMxwk7HaoZchR8E). Accessed 1 June 2021
- Anuradha J, Abbasi T, Abbasi SA (2015) An eco-friendly method of synthesizing gold nanoparticles using an otherwise worthless weed pistia (*Pistia stratiotes* L.). *J. Adv. Res.* 6:711–720. <https://doi.org/10.1016/j.jare.2014.03.006>
- Arbab Zavar MH, Heydari S, Rounaghi GH, Eshghi H, Azizi-Toupanloo H (2012) Electrochemical behavior of para-nitroaniline at a new synthetic crown ether-silver nanoparticle modified carbon paste electrode. *Anal Methods* 4:953–958. <https://doi.org/10.1039/c2ay05892h>
- Arulraj AD, Vijayan M, Vasanth VS (2015) Highly selective and sensitive simple sensor based on electrochemically treated nano polypyrrole-sodium dodecyl sulphate film for the detection of para-nitrophenol. *Anal Chim Acta* 899:66–74. <https://doi.org/10.1016/j.aca.2015.09.055>
- Balasubramanian P, Balamurugan TST, Chen SM, Chen TW (2019) Simultaneous synthesis of ultrafine  $\text{CoMnO}_3$  nanosheets: An excellent electrocatalyst for highly sensitive detection of toxic 4-nitrophenol in environmental water samples. *J Hazard Mater* 361:123–133. <https://doi.org/10.1016/j.jhazmat.2018.08.070>
- Basavegowda N, Mishra K, Lee YR (2014) Sonochemically synthesized ferromagnetic  $\text{Fe}_3\text{O}_4$  nanoparticles as a recyclable catalyst for the preparation of pyrrolo[3,4-c]quinoline-1,3-dione derivatives. *RSC Adv* 4:61660–61666. <https://doi.org/10.1039/C4RA11623B>
- Belloli R, Barletta B, Bolzacchini E, Meinardi S, Orlandi M, Rindone B (1999) Determination of toxic nitrophenols in the atmosphere by high-performance liquid chromatography. *J Chromatogr A* 846:277–281. [https://doi.org/10.1016/S0021-9673\(99\)00030-8](https://doi.org/10.1016/S0021-9673(99)00030-8)
- Busca G, Berardinelli S, Resini C, Arrighi L (2008) Technologies for the removal of phenol from fluid streams: A short review of recent developments. *J Hazard Mater* 160:265–288. <https://doi.org/10.1016/j.jhazmat.2008.03.045>
- Calam TT (2020) Electrochemical oxidative determination and electrochemical behavior of 4-nitrophenol based on an au electrode modified with electro-polymerized 3,5-diamino-1,2,4-triazole film. *Electroanalysis* 32:149–158. <https://doi.org/10.1002/elan.201900450>
- Caruso F (2001) Nanoengineering of Particle Surfaces. *Adv Mater* 13:11–22. [https://doi.org/10.1002/1521-4095\(200101\)13:1%3c11::AID-ADMA11%3e3.0.CO;2-N](https://doi.org/10.1002/1521-4095(200101)13:1%3c11::AID-ADMA11%3e3.0.CO;2-N)
- Castañeda C, Tzompantzi F, Gómez R (2016) Photocatalytic reduction of 4-nitrophenol on in situ fluorinated sol–gel

- TiO<sub>2</sub> under UV irradiation using Na<sub>2</sub>SO<sub>3</sub> as reducing agent. *J Sol-Gel Sci Technol* 80:426–435. <https://doi.org/10.1007/s10971-016-4104-2>
- Chen B, Huang W (2009) Effect of background electrolytes on the adsorption of nitroaromatic compounds onto bentonite. *J Environ Sci* 21:1044–1052. [https://doi.org/10.1016/S1001-0742\(08\)62380-3](https://doi.org/10.1016/S1001-0742(08)62380-3)
- Chevallier A (1996) *The Encyclopedia of medicinal plants an excellent guide to over 500 of the more well-known medicinal herbs from around the world*. Dorling Kindersley, London. - References - Scientific Research Publishing, (n.d.). [https://www.scirp.org/\(S\(i43dy n45teexjx455q1t3d2q\)\)/reference/ReferencesPapers.aspx?ReferenceID=1333491](https://www.scirp.org/(S(i43dy n45teexjx455q1t3d2q))/reference/ReferencesPapers.aspx?ReferenceID=1333491) (accessed June 1, 2021).
- Chu L, Han L, Zhang X (2011) Electrochemical simultaneous determination of nitrophenol isomers at nano-gold modified glassy carbon electrode. *J Appl Electrochem* 41:687–694. <https://doi.org/10.1007/s10800-011-0281-4>
- De Lima CA, Da Silva PS, Spinelli A (2014) Chitosan-stabilized silver nanoparticles for voltammetric detection of nitrocompounds. *Sensors Actuators, B Chem* 196:39–45. <https://doi.org/10.1016/j.snb.2014.02.005>
- de Valber A, Pedrosa LC, Avaca LA (2003) Electroanalytical determination of 4-nitrophenol by square wave voltammetry on diamond electrodes. *J Braz Chem Soc* 14(4):530–535. <https://doi.org/10.1590/S0103-50532003000400007>
- Devatha CP, Jagadeesh K, Patil M (2018) Effect of Green synthesized iron nanoparticles by *Azadirachta indica* in different proportions on antibacterial activity. *Environ. Nanotechnology. Monit Manag* 9:85–94. <https://doi.org/10.1016/j.enmm.2017.11.007>
- Ebrahimzadeh H, Yamini Y, Kamarei F (2009) Optimization of dispersive liquid-liquid microextraction combined with gas chromatography for the analysis of nitroaromatic compounds in water. *Talanta* 79:1472–1477. <https://doi.org/10.1016/j.talanta.2009.06.022>
- Elemike EE, Onwudiwe DC, Nundkumar N, Singh M, Iyekowa O (2019) Green synthesis of Ag, Au and Ag-Au bimetallic nanoparticles using *Stigmaphyllon ovatum* leaf extract and their in vitro anticancer potential. *Mater Lett* 243:148–152. <https://doi.org/10.1016/j.matlet.2019.02.049>
- Erkan G, Şengül K, Kaya S (2014) Dyeing of white and indigo dyed cotton fabrics with *Mimosa tenuiflora* extract. *J Saudi Chem Soc* 18:139–148. <https://doi.org/10.1016/j.jscs.2011.06.001>
- Feng X, Mao C, Yang G, Hou W, Zhu JJ (2006) Polyaniline/Au composite hollow spheres: Synthesis, characterization, and application to the detection of dopamine. *Langmuir* 22:4384–4389. <https://doi.org/10.1021/la053403r>
- Garbellini GS, Salazar-Banda GR, Avaca LA (2007) Sonovoltammetric determination of 4-nitrophenol on diamond electrodes. *J Braz Chem Soc* 18:1095–1099. <https://doi.org/10.1590/S0103-50532007000600002>
- German N, Ramanaviciene A, Ramanavicius A (2019) Formation of polyaniline and polypyrrole nanocomposites with embedded glucose oxidase and gold nanoparticles. *Polymers (basel)* 11:377. <https://doi.org/10.3390/polym11020377>
- German N, Ramanaviciene A, Ramanavicius A (2020) Formation and electrochemical evaluation of polyaniline and polypyrrole nanocomposites based on glucose oxidase and gold nanostructures. *Polymers (basel)* 12:3026. <https://doi.org/10.3390/polym12123026>
- German N, Ramanaviciene A, Ramanavicius A (2021) Dispersed conducting polymer nanocomposites with glucose oxidase and gold nanoparticles for the design of enzymatic glucose biosensors. *Polymers (basel)* 13:2173. <https://doi.org/10.3390/polym13132173>
- Ghanbari D, Salavati-Niasari M, Ghasemi-Kooch M (2014) A sonochemical method for synthesis of Fe<sub>3</sub>O<sub>4</sub> nanoparticles and thermal stable PVA-based magnetic nanocomposite. *J Ind Eng Chem* 20:3970–3974. <https://doi.org/10.1016/J.JIEC.2013.12.098>
- Gonçalves LM, Batchelor-McAuley C, Barros AA, Compton RG (2010) Electrochemical oxidation of adenine: A mixed adsorption and diffusion response on an edge-plane pyrolytic graphite electrode. *J Phys Chem C* 114(33):14213–14219. <https://doi.org/10.1021/jp1046672>
- Grieve, A *Modern Herbal*, Penguin 1984, n.d.
- Guidotti M, Ravaioli G, Vitali M (1999) Total p-nitrophenol determination in urine samples of subjects exposed to parathion and methyl-parathion by SPME and GC/MS HRC. *J High Resolut Chromatogr* 22:628–630
- Guo X, Wang Z, Zhou S (2004) The separation and determination of nitrophenol isomers by high-performance capillary zone electrophoresis. *Talanta* 64:135–139. <https://doi.org/10.1016/j.talanta.2004.01.020>
- Hofmann D, Hartmann F, Herrmann H (2008) Analysis of nitrophenols in cloud water with a miniaturized light-phase rotary perforator and HPLC-MS. *Anal Bioanal Chem* 391:161–169. <https://doi.org/10.1007/s00216-008-1939-6>
- Hu G, Guo Y, Shao S (2009) Simultaneous determination of dopamine and ascorbic acid using the nano-gold self-assembled glassy carbon electrode. *Electroanalysis* 21:1200–1206. <https://doi.org/10.1002/elan.200804510>
- Jiang P, Zhou J, Zhang A, Zhong Y (2010) Electrochemical degradation of p-nitrophenol with different processes. *J Environ Sci* 22:500–506. [https://doi.org/10.1016/S1001-0742\(09\)60140-6](https://doi.org/10.1016/S1001-0742(09)60140-6)
- Jiao XX, Luo HQ, Li NB (2013) Fabrication of graphene-gold nanocomposites by electrochemical co-reduction and their electrocatalytic activity toward 4-nitrophenol oxidation. *J Electroanal Chem* 691:83–89. <https://doi.org/10.1016/J.JELECHEM.2012.12.013>
- Kamei K, Mukai Y, Kojima H, Yoshikawa T, Yoshikawa M, Kiyohara G, Yamamoto TA, Yoshioka Y, Okada N, Seino S, Nakagawa S (2009) Direct cell entry of gold/iron-oxide magnetic nanoparticles in adenovirus mediated gene delivery. *Biomaterials* 30:1809–1814. <https://doi.org/10.1016/j.biomaterials.2008.12.015>
- Karuppiyah C, Palanisamy S, Chen SM, Emmanuel R, Ali MA, Muthukrishnan P, Prakash P, Al-Hemaid FMA (2014) Green biosynthesis of silver nanoparticles and nanomolar detection of p-nitrophenol. *J Solid State Electrochem* 18:1847–1854. <https://doi.org/10.1007/s10008-014-2425-z>
- Khan SB, Akhtar K, Bakhsh EM, Asiri AM (2019) Electrochemical detection and catalytic removal of 4-nitrophenol using CeO<sub>2</sub>-Cu<sub>2</sub>O and CeO<sub>2</sub>-Cu<sub>2</sub>O/CH nanocomposites. *Appl Surf Sci* 492:726–735. <https://doi.org/10.1016/j.apsusc.2019.06.205>
- Khatoun UT, Rao GVS, Mohan MK, Ramanaviciene A, Ramanavicius A (2018) Comparative study of antifungal activity of silver and gold nanoparticles synthesized by facile chemical approach. *J Environ Chem Eng* 6:5837–5844. <https://doi.org/10.1016/j.jece.2018.08.009>
- Kojima H, Mukai Y, Yoshikawa M, Kamei K, Yoshikawa T, Morita M, Inubushi T, Yamamoto TA, Yoshioka Y, Okada N, Seino S, Nakagawa S (2010) Simple PEG conjugation of SPIO via an Au-S bond improves its tumor targeting potency as a novel MR tumor imaging agent. *Bioconjug Chem* 21:1026–1031. <https://doi.org/10.1021/bc900487p>
- Kotyuk LA (2015) Hyssop composition depending on age and plants development phases. *Biotechnologia Acta* 8(5):55–63. <https://doi.org/10.15407/biotech8.05.055>
- Kumar KM, Mandal BK, Kumar KS, Reddy PS, Sreedhar B (2013) Biobased green method to synthesise palladium and iron nanoparticles using *Terminalia chebula* aqueous extract. *Spectrochim Acta Part A: Mol Biomol Spectrosc* 102:128–133. <https://doi.org/10.1016/j.saa.2012.10.015>
- Leung KCF, Xuan S, Zhu X, Wang D, Chak CP, Lee SF, Ho KW, Chung BCT (2012) Gold and iron oxide hybrid nanocomposite materials. *Chem Soc Rev* 41:1911–1928. <https://doi.org/10.1039/c1cs15213k>

- Li X, Wan M, Wei Y, Shen J, Chen Z (2006) Electromagnetic functionalized and core-shell micro/nanostructured polypyrrole composites. *J Phys Chem B* 110:14623–14626. <https://doi.org/10.1021/jp062339z>
- Li S, Du D, Huang J, Tu H, Yang Y, Zhang A (2013) One-step electro-deposition of a molecularly imprinting chitosan/ phenyltrimethoxysilane/AuNPs hybrid film and its application in the selective determination of p-nitrophenol. *Analyst* 138:2761–2768. <https://doi.org/10.1039/c3an36497f>
- Lipczynska-Kochany E (1991) Degradation of aqueous nitrophenols and nitrobenzene by means of the Fenton reaction. *Chemosphere* 22:529–536. [https://doi.org/10.1016/0045-6535\(91\)90064-K](https://doi.org/10.1016/0045-6535(91)90064-K)
- Luo F, Chen Z, Megharaj M, Naidu R (2014) Biomolecules in grape leaf extract involved in one-step synthesis of iron-based nanoparticles. *RSC Adv* 4:53467–53474. <https://doi.org/10.1039/C4RA08808E>
- M. Mahdavi, F. Namvar, M. Bin Ahmad, R. Mohamad, Green Biosynthesis and Characterization of Magnetic Iron Oxide (Fe<sub>3</sub>O<sub>4</sub>) Nanoparticles Using Seaweed (*Sargassum muticum*) Aqueous Extract, *Mol. 2013, Vol. 18, Pages 5954–5964*. 18 (2013) 5954–5964. <https://doi.org/10.3390/MOLECULES18055954>.
- Mansoureh G, Parisa V (2018) Synthesis of metal nanoparticles using laser ablation technique. *Emerging Applications of Nanoparticles and Architecture Nanostructures*. Elsevier, pp 575–596. <https://doi.org/10.1016/B978-0-323-51254-1.00019-1>
- Mareedu T, Poiba V, Vangalapati M (2021) Green synthesis of iron nanoparticles by green tea and black tea leaves extract. *Mater Today Proc* 42:1498–1501. <https://doi.org/10.1016/J.MATPR.2021.01.444>
- Mojović Z, Petrović S, Mojović M, Pavlović S, Rožić L (2021) Ruthenium containing perovskites as electrode materials for 4-nitrophenol detection. *J Phys Chem Solids* 148:109649. <https://doi.org/10.1016/j.jpccs.2020.109649>
- Mußmann P, Levsen K, Radeck W (1994) Gas-chromatographic determination of phenols in aqueous samples after solid phase extraction, *Fresenius. J Anal Chem* 348:654–659. <https://doi.org/10.1007/BF00325568>
- Nash MA, Yager P, Hoffman AS, Stayton PS (2010) Mixed stimuli-responsive magnetic and gold nanoparticle system for rapid purification, enrichment, and detection of biomarkers. *Bioconjug Chem* 21:2197–2204. <https://doi.org/10.1021/bc100180q>
- Nasrollahzadeh M, Sajadi SM (2016) Preparation of Pd/Fe<sub>3</sub>O<sub>4</sub> nanoparticles by use of *Euphorbia stracheyi* Boiss root extract: a magnetically recoverable catalyst for one-pot reductive amination of aldehydes at room temperature. *J Colloid Interface Sci* 464:147–152. <https://doi.org/10.1016/J.JCIS.2015.11.020>
- Niazi A, Yazdanipour A (2007) Spectrophotometric simultaneous determination of nitrophenol isomers by orthogonal signal correction and partial least squares. *J Hazard Mater* 146:421–427. <https://doi.org/10.1016/j.jhazmat.2007.03.063>
- Ojea-Jiménez I, Campanera JM (2012) Molecular modeling of the reduction mechanism in the citrate-mediated synthesis of gold nanoparticles. *J Phys Chem C* 116:23682–23691. <https://doi.org/10.1021/JP305830P>
- Oliveira-Filho GB, Atoche-Medrano JJ, Aragón FFH, Mantilla Ochoa JC, Pacheco-Salazar DG, da Silva SW, Coaquira JAH (2021) Core-shell Au/Fe<sub>3</sub>O<sub>4</sub> nanocomposite synthesized by thermal decomposition method: Structural, optical, and magnetic properties. *Appl Surf Sci*. <https://doi.org/10.1016/j.apsusc.2021.150290>
- Pong B-K, Elim HI, Chong J-X, Ji W, Trout BL, Lee J-Y (2007) New insights on the nanoparticle growth mechanism in the citrate reduction of gold(III) salt: formation of the au nanowire intermediate and its nonlinear optical properties. *J Phys Chem C* 111(17):6281–6287. <https://doi.org/10.1021/jp068666o>
- Predescu AM, Matei E, Berbecaru AC, Pantilimon C, Drăgan C, Vidu R, Predescu C, Kuncser V (2018) Synthesis and characterization of dextran-coated iron oxide nanoparticles. *R Soc Open Sci*. <https://doi.org/10.1098/RSOS.171525>
- Ramalingam M, Ponnusamy VK, Sangilimuthu SN (2020) Electrochemical determination of 4-nitrophenol in environmental water samples using porous graphitic carbon nitride-coated screen-printed electrode. *Environ Sci Pollut Res* 27:17481–17491. <https://doi.org/10.1007/s11356-019-05494-3>
- Ramanaviciene A, Voronovic J, Popov A, Drevinskas R, Kausaite-Minkstimiene A, Ramanavicius A (2016) Investigation of biocatalytic enlargement of gold nanoparticles using dynamic light scattering and atomic force microscopy. *Colloids Surf A Physicochem Eng Asp* 510:183–189. <https://doi.org/10.1016/j.colsurfa.2016.07.078>
- Ramanaviciene A, German N, Kausaite-Minkstimiene A, Ramanavicius A (2021) Glucose biosensor based on dendritic gold nanostructures electrodeposited on graphite electrode by different electrochemical methods. *Chemosensors* 9:188. <https://doi.org/10.3390/chemosensors9080188>
- Ramanavicius A, German N, Ramanaviciene A (2017) Evaluation of electron transfer in electrochemical system based on immobilized gold nanoparticles and glucose oxidase. *J Electrochem Soc* 164:G45–G49. <https://doi.org/10.1149/2.0691704jes>
- Roca M, Haes AJ (2008) Silica-void-gold nanoparticles: Temporally stable surface-enhanced raman scattering substrates. *J Am Chem Soc* 130:14273–14279. <https://doi.org/10.1021/ja8059039>
- Rodríguez-León E, Rodríguez-Vázquez BE, Martínez-Higuera A, Rodríguez-Beas C, Larios-Rodríguez E, Navarro RE, López-Esparza R, Iñiguez-Palomares RA (2019) Synthesis of gold nanoparticles using mimosa tenuiflora extract, assessments of cytotoxicity, cellular uptake, and catalysis. *Nanoscale Res Lett*. <https://doi.org/10.1186/s11671-019-3158-9>
- Rosli IR, Zulhaimi HI, Ibrahim SKM, Gopinath SCB, Kasim KF, Akmal HM, Nuradibah MA, Sam TS, Rosli IR, Zulhaimi HI, Ibrahim SKM, Gopinath SCB, Kasim KF, Akmal HM, Nuradibah MA, Sam TS (2018) Phytosynthesis of iron nanoparticle from *averrhoa bilimbi* linn. *Molecules*. <https://doi.org/10.1088/1757-899X/318/1/012012>
- Sacara AM, Cristea C, Muresan LM (2017) Electrochemical detection of Malachite Green using glassy carbon electrodes modified with CeO<sub>2</sub> nanoparticles and Nafion. *J Electroanal Chem* 792:23–30. <https://doi.org/10.1016/j.jelechem.2017.03.030>
- Saif S, Tahir A, Asim T, Chen Y, Adil S (2019) Polymeric Nanocomposites of Iron-Oxide Nanoparticles (IONPs) Synthesized Using Terminalia chebula Leaf Extract for Enhanced Adsorption of Arsenic(V) from Water. *Colloids and Interfaces* 3:17. <https://doi.org/10.3390/colloids3010017>
- Salaheldin HI (2017) Comparative catalytic reduction of 4-nitrophenol by polyacrylamide-gold nanocomposite synthesized by hydrothermal autoclaving and conventional heating routes. *Adv Nat Sci Nanosci Nanotechnol*. <https://doi.org/10.1088/2043-6254/aa8542>
- Salgueiriño-Maceira V, Correa-Duarte MA, Spasova M, Liz-Marzán LM, Farle M (2006) Composite Silica Spheres with Magnetic and Luminescent Functionalities. *Adv Funct Mater* 16:509–514. <https://doi.org/10.1002/adfm.200500565>
- Shan F, Zhang T (2018) Theoretical study on surface plasmon properties of gold nanostars. *IOP Conf Ser Mater Sci Eng* 322:022005. <https://doi.org/10.1088/1757-899X/322/2/022005>
- Sheikh L, Sinha S, Singhababu YN, Verma V, Tripathy S, Nayar S (2018) Traversing the profile of biomimetically nanoengineered iron substituted hydroxyapatite: synthesis, characterization, property evaluation, and drug release modeling. *RSC Adv* 8:19389–19401. <https://doi.org/10.1039/c8ra01539b>
- Sittig's Handbook of Toxic and Hazardous Chemicals and Carcinogens - 6th Edition, (n.d.). <https://www.elsevier.com/books/sittigs-handbook-of-toxic-and-hazardous-chemicals-and-carcinogens/pohanish/978-1-4377-7869-4> (accessed May 19, 2021).

- Tang Y, Huang R, Liu C, Yang S, Lu Z, Luo S (2013) Electrochemical detection of 4-nitrophenol based on a glassy carbon electrode modified with a reduced graphene oxide/Au nanoparticle composite. *Anal Methods* 5:5508–5514. <https://doi.org/10.1039/c3ay40742j>
- Thompson MJ, Ballinger LN, Cross SE, Roberts MS (1996) High-performance liquid chromatographic determination of phenol, 4-nitrophenol,  $\beta$ -naphthol and a number of their glucuronide and sulphate conjugates in organ perfusate. *J Chromatogr B Biomed Appl* 677:117–122. [https://doi.org/10.1016/0378-4347\(95\)00368-1](https://doi.org/10.1016/0378-4347(95)00368-1)
- Wang Z (2013) Iron Complex Nanoparticles Synthesized by Eucalyptus Leaves. *ACS Sustain Chem Eng* 1:1551–1554. <https://doi.org/10.1021/SC400174A>
- Wang J, Liu J, Guo X, Yan L, Lincoln SF (2016) The formation and catalytic activity of silver nanoparticles in aqueous polyacrylate solutions. *Front Chem Sci Eng* 10:432–439. <https://doi.org/10.1007/s11705-016-1584-0>
- Wei Y, Kong LT, Yang R, Wang L, Liu JH, Huang XJ (2011) Single-walled carbon nanotube/pyrenecyclodextrin nanohybrids for ultrahighly sensitive and selective detection of p-nitrophenol. *Langmuir* 27:10295–10301. <https://doi.org/10.1021/la201691c>
- Wiench P, Grzyb B, González Z, Menéndez R, Handke B, Gryglewicz G (2017) pH robust electrochemical detection of 4-nitrophenol on a reduced graphene oxide modified glassy carbon electrode. *J Electroanal Chem* 787:80–87. <https://doi.org/10.1016/j.jelechem.2017.01.040>
- Wong JM, Li QX, Hammock BD, Seiber JN (1991) Method for the analysis of 4-nitrophenol and parathion in soil using supercritical fluid extraction and immunoassay. *J Agric Food Chem* 39:1802–1807. <https://doi.org/10.1021/jf00010a022>
- Yadav VK, Ali D, Khan SH, Gnanamoorthy G, Choudhary N, Yadav KK, Thai VN, Hussain SA, Manhrdas S (2020) Synthesis and characterization of amorphous iron oxide nanoparticles by the sonochemical method and their application for the remediation of heavy metals from wastewater. *Nanomaterials* 10:1551. <https://doi.org/10.3390/nano10081551>
- Yang L, Fan S, Deng G, Li Y, Ran X, Zhao H, Li CP (2015) Bridged  $\beta$ -cyclodextrin-functionalized MWCNT with higher supramolecular recognition capability: The simultaneous electrochemical determination of three phenols. *Biosens Bioelectron* 68:617–625. <https://doi.org/10.1016/j.bios.2015.01.059>
- Yew YP, Shameli K, Miyake M, Ahmad Khairudin NBB, Mohamad SEB, Naiki T, Lee KX (2020) Green biosynthesis of superparamagnetic magnetite Fe<sub>3</sub>O<sub>4</sub> nanoparticles and biomedical applications in targeted anticancer drug delivery system: A review. *Arab J Chem* 13:2287–2308. <https://doi.org/10.1016/J.ARABJC.2018.04.013>
- Yi DK, Lee SS, Ying JY (2006) Synthesis and applications of magnetic nanocomposite catalysts. *Chem Mater* 18:2459–2461. <https://doi.org/10.1021/cm052885p>
- Yin H, Zhou Y, Ai S, Ma Q, Zhu L, Lu L (2012) Electrochemical oxidation determination and voltammetric behaviour of 4-nitrophenol based on Cu<sub>2</sub>O nanoparticles modified glassy carbon electrode. *Int J Environ Anal Chem* 92:742–754. <https://doi.org/10.1080/03067319.2010.520123>
- Zayed MF, Eisa WH (2014) Phoenix dactylifera L. leaf extract phytosynthesized gold nanoparticles; Controlled synthesis and catalytic activity, *Spectrochim. Acta - Part A Mol. Biomol Spectrosc* 121:238–244. <https://doi.org/10.1016/j.saa.2013.10.092>
- Zhao G-H, Tang Y-T, Liu M-C, Lei Y-Z, Xiao X-E (2007) Direct and simultaneous determination of phenol, hydroquinone and nitrophenol at boron-doped diamond film electrode. *Chinese J Chem* 25:1445–1450. <https://doi.org/10.1002/cjoc.200790267>
- Zhao P, Feng X, Huang D, Yang G, Astruc D (2015) Basic concepts and recent advances in nitrophenol reduction by gold- and other transition metal nanoparticles. *Coord Chem Rev* 287:114–136. <https://doi.org/10.1016/j.ccr.2015.01.002>

**Publisher's Note** Springer Nature remains neutral with regard to jurisdictional claims in published maps and institutional affiliations.

## Authors and Affiliations

Aisha A. Ganash<sup>1</sup>  · Rahmah A. Aljubairy<sup>1</sup>

✉ Aisha A. Ganash  
aganash@kau.edu.sa

<sup>1</sup> Chemistry Department, Faculty of Science, King Abdulaziz University, Jeddah, Saudi Arabia